Cracking in Drying Latex Films

ARTICLE *in* LANGMUIR · JUNE 2005

Impact Factor: 4.46 · DOI: 10.1021/la048298k · Source: PubMed

Cracking in Drying Latex Films

Mahesh S. Tirumkudulu*

Department of Chemical Engineering, Indian Institute of Technology-Bombay, Mumbai 400076, India

William B. Russel

Department of Chemical Engineering, Princeton University, New Jersey 08544

Received July 7, 2004. In Final Form: January 7, 2005

Thin films of latex dispersions containing particles of high glass transition temperature generally crack while drying under ambient conditions. Experiments with particles of varying radii focused on conditions for which capillary stresses normal to the film deform the particles elastically and generate tensile stresses in the plane of the film. Irrespective of the particle size, the drying film contained, simultaneously, domains consisting of a fluid dispersion, a fully dried packing of deformed spheres, and a close packed array saturated with water. Interestingly, films cast from dispersions containing 95-nm sized particles developed tensile stresses and ultimately became transparent even in the absence of water, indicating that van der Waals forces can deform the particles. Employing the stress−strain relation for a drying latex film along with the well-known Griffith's energy balance concept, we calculate the critical stress at cracking and the accompanying crack spacing, in general agreement with the observed values.

1. Introduction

When a thin film of a latex dispersion containing soft polymer particles, such as a wet paint, is applied on a nonporous surface, evaporation of the solvent concentrates the particles into a close packed array. Further evaporation is accompanied by stresses in the wet film that deform the particles so as to close the pores. When the particle glass transition temperature is sufficiently lower than the ambient temperature, polymer chains diffuse across contacting interfaces to fuse the particles, ultimately resulting in a homogeneous film. The film generally binds to the underlying substrate, generating shear stresses that resist deformation in the transverse plane and giving rise to transverse tensile stresses. When the magnitude of the tensile stress exceeds a critical value, cracks nucleate, thereby compromising the mechanical integrity of the film. Recent developments in the understanding of the film formation process have shown the drying and particle deformation mechanisms to be rather complex and not completely understood.

In a review, Holl et al.[1] distinguish three different modes of drying in a wet film. The first mode, which is rarely observed, corresponds to homogeneous drying where the water concentration is spatially homogeneous and all parts of the film dry at the same rate. The second mode of drying occurs when the particle diffusivity is negligible, allowing evaporation to concentrate particles at the liquid−air interface. The resulting "sheet" of packed particles at the surface grows in thickness as the vertical convection induced by the negative capillary pressure draws in more particles. Here, the capillary pressure is caused by the liquid menisci between the particles at the air−film interface. Finally, the third mode involving propagation of lateral fronts occurs when the nonuniform thickness of the film causes the particles to reach close packing first at the edge. Here, in contrast to the previous case, the low pressure caused by the liquid menisci at the edge draws water laterally from the bulk and deposits particles at the front. In a variation on this theme for a drying liquid drop, Deegan et al.[2] suggested that a pinned liquid−solid contact line at the edge would induce bulk flow to the edge, to maintain a constant contact angle. They also noted that the local evaporation rate varies spatially with the highest rates observed at the edges, exacerbating the effects.

The evaporation of solvent from a film of close packed particles can cause particle deformation. The earliest theory of deformation for spheres in contact, proposed by Hertz,[3] relates the change in the center to center distance between two touching spheres to their elastic modulus and the external force squeezing them together. In contrast, the viscous sintering of two spheres, proposed by Frenkel,[4] balances the interfacial tension (γ), which minimizes the particle surface area, against viscous forces resisting deformation, resulting in a simple relation between rate of strain, the internal viscosity of the particle, and interfacial tension. Finally, the JKR[5] theory balances the surface energy and elastic response to predict the strain as a function of the interfacial tension and the shear modulus. Routh and Russel,[6] henceforth referred to as RR, recently consolidated the various theories by considering the viscoelastic deformation of a pair of particles due to both interfacial tension and external forces such as those exerted by neighbors in contact. They volume average the stress within the particles to relate the forces acting on the pair to the deformation and then ensemble average the force dipoles in the particle pairs to arrive at a macroscopic stress−strain relation for a deforming film. This differs from the classical approaches of Biot[7] and

(1) Holl, Y.; Keddie, J. L.; McDonald, P.; Winnik, W. In *Film formation in coatings: Mechanisms, Properties and Morphology*; Provder, T., Urban, M. W., Eds.; ACS Symposium Series 790; Amercian Chemical Society: Washington, DC, 2001; Chapter 1, pp 2−26.

(2) Deegan, R. D.; Bakajin, O.; Dupont, T.; Huber, G.; Nagel, S.; Witten, T. *Nature* **1997**, *389*, 827−829.

(3) Maugis, D. *Contact, Adhesion and Rupture of Elastic Solids*; Springer: New York, 1999.

(4) Frenkel, J. *J. Phys.* **1945**, *9*, 385.

(5) Johnson, K.; Kendall, K.; Roberts, A. *Proc. R. Soc. London, Ser. A* **1971**, *324*, 301−313.

(6) Routh, A. F.; Russel, W. B. *Langmuir* **1999**, *15* (22), 7762−7773.

(7) Biot, M. *J. Appl. Mech.* **1956**, *23*, 91−96.

10.1021/la048298k CCC: $30.25
Published on Web 04/29/2005

others in recognizing the intrinsically nonlinear response of spheres in contact. They then coupled evaporation with particle deformation and predicted the lateral front propagation in a drying film.[8]

Although cracking during drying of wet films is observed for diverse systems such as wet clays, ceramics slips, and model colloidal dispersions,[9−13] the experiments of Cima and co-workers[14,15] appear to be the most relevant to the current study. They report drying and the accompanying cracking in wet ceramic films prepared from electrostatically stabilized suspensions of α-alumina particles of 200 and 400 nm diameter in water. Photographs of drying alumina films showed three different domains: a central super-saturated region containing the fluid dispersion, an outer dry film, and an intermediate saturated domain containing closely packed particles saturated with water. As evaporation proceeded, the "wet" and "dry" fronts, which refer to respectively the fronts separating the super-saturated and saturated domains and saturated and dry domains, advanced from all sides toward the center of the film. The cracks were observed to nucleate at some distance from the edge of the film and were oriented perpendicular to the moving fronts. Interestingly, the cracks extended into the saturated region and propagated with the moving fronts toward the center of the film. From experiments on films of various thicknesses, they determined a critical cracking thickness (CCT) above which films would crack spontaneously. The CCT was observed to increase with increasing particle size suggesting that films formed from large particles are less likely to crack. Films cast on a pool of mercury resulted in a much higher CCT indicating that the tensile stress induced during drying is directly related to the constraint imposed by the underlying substrate. These experiments were followed by measurements of tensile stresses using the substrate deflection method based on an optical interference technique. The magnitude of the tensile stresses was found to scale on the capillary pressure (based on the particle size), demonstrating the induced tensile stresses to be caused by liquid menisci formed between neighboring particles in a packed particle array.

There have been two main approaches to the theoretical description of cracking in drying films. A statistical description for the fracture process, adopted first by Meakin,[9,16] considers a monolayer of closely packed particles that are bonded to each other and to the underlying substrate via elastic springs. Starting from an uniformly stressed film, the bonds (or springs) between the particles are broken at random with an assumed probability, following which the system is allowed to relax to a new equilibrium. On repeating the above process a number of times, crack patterns emerge that closely resemble those observed experimentally. The second approach, which will be followed here, views the material as a continuum and assumes a macroscopic model for the stress−strain relation of an elastic material. Using simple energy balances (e.g., Griffith's concept[17]), a criterion for fracture is derived on the basis of specimen geometry and external loads.[18−20]

In this study, we report the stresses generated during drying and the accompanying cracking behavior for latex dispersions containing particles of varying radii. Using the Griffith's criterion for equilibrium crack propagation along with the stress−strain relation developed by Routh and Russel[6] for drying films, we compare the stress at crack nucleation and the resulting crack spacing to that observed experimentally and find a clear correspondence.

Table 1. Details of the Dispersions Used in the Experiments[a]

dispersion	particle composition	particle diameter (nm)	T_g (°C)	G (MPa)
PPG342	PS	342	100	4200
GMA610	PS core, PMMA/GMA shell	610	65−80	1700
PMMA95	PMMA	95	105	1700

[a] To calculate the critical stress and crack spacing, the number of close neighbors, M, was assigned a value of 6 which is the number of neighbors in contact to immobilize close packed spheres.[28] Previously,[24] these parameter values resulted in stress profiles in close agreement with measurements.

2. Materials and Experimental Technique

The stress development during drying and the accompanying cracking were observed experimentally by casting thin films of latex dispersions on copper substrates. A few experiments were also performed on glass slides in order to observe debonding from the underside. Three different aqueous dispersions containing polymer spheres of diameters 95, 342, and 610 nm were utilized. Since the glass transition temperature of the polymers was much higher than the experimental ambient temperature, cracking was observed in films cast from all the three dispersions. The details of the aqueous dispersions are listed in Table 1.

The stresses were measured according to the classical cantilever technique,[21,22] in which a thin wet film of dispersion dries on an elastic substrate. The stresses generated in the plane of the film during drying can be deduced from the deflection of the substrate. Since our experimental setup is similar to that employed by Petersen et al.[23] and has been described earlier,[24] only a brief description will be given here. Thin films of dispersions were applied on rectangular strips of copper of mean thickness 76 μm and Young's modulus 117 GPa. One end of the substrate was clamped while a small mirror (mylar) was glued to the other (free) end. A laser beam incident on the mirror was collected, on reflection, by a position sensitive detector. Care was taken to ensure that the reflected beam was perpendicular to the detector surface. The signals from the detector along with those from a temperature and humidity sensor, placed in the vicinity of the drying film, were acquired at intervals of 0.1 s by a computer. The entire setup was enclosed in a Plexiglas chamber to prevent air circulation from affecting the experiments. The experiments were conducted over a range of temperatures (19−24 °C) and relative humidities (30−70%). Evaporation rates were determined separately, under the same ambient conditions, by recording the weight of wet films on a balance as a function of time.

The bulk stress σ_o in the plane of the film can be determined from the well-known plate/beam deflection relation,[23]

$$\sigma_o = \frac{E_s t_s^3}{6 t_f (t_s + t_f)} \frac{\theta}{l_f} \quad (1)$$

(8) Routh, A.; Russel, W.; Tang, J.; El-Aassser, M. S. *J. Coat. Technol.* **2001**, *73* (916), 41−48.
(9) Skjeltorp, A. T.; Meakin, P. *Nature* **1988**, *335*, 424−426.
(10) Allain, C.; Limat, L. *Phys. Rev. Lett.* **1995**, *74* (15), 2981−2984.
(11) Pauchard, L.; Parisse, F.; Allain, C. *Phys. Rev. E* **1999**, *59* (3), 3737−3740.
(12) Colina, H.; Roux, S. *Eur. Phys. J. E* **2000**, *1*, 189−194.
(13) Shorlin, K.; de Bruyn, J.; Graham, M.; Morris, S. *Phys. Rev. E* **2000**, *61* (6), 6950−6957.
(14) Chiu, R.; Garino, T.; Cima, M. *J. Am. Ceram. Soc.* **1993**, *76* (9), 2257−2264.
(15) Chiu, R.; Cima, M. *J. Am. Ceram. Soc.* **1993**, *76* (11), 2769−2777.
(16) Meakin, P. *Thin Solid Films* **1987**, *151* (2), 165−190.
(17) Lawn, B. *Fracture of Brittle Solids*, 2nd ed.; Cambridge University Press: New York, 1993.
(18) Beuth, J. L., Jr. *Int. J. Solids Struct.* **1992**, *29* (13), 1657−1675.
(19) Xia, Z.; Hutchinson, J. *J. Mech. Phys. Solids* **2000**, *48*, 1107−1131.
(20) Jagota, A.; Hui, C. Y. *Mech. Mater.* **1991**, *11* (3), 221−234.
(21) Corcoran, E. *J. Paint Technol.* **1969**, *41* (538), 635−640.
(22) Perera, D.; Eynde, D. *J. Coat. Technol.* **1981**, *53* (677), 39−44.

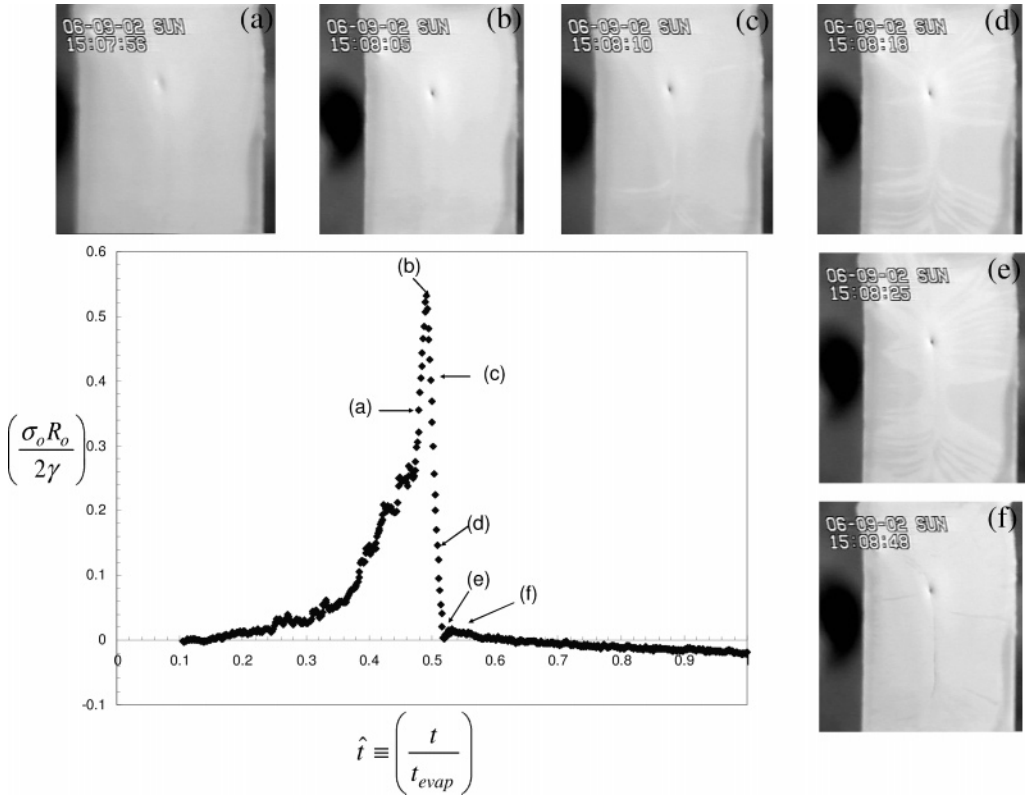

Figure 1. Plot of the dimensionless stress measured for a PPG342 dispersion of $\phi_o = 0.38$, as a function of dimensionless time. A wet film of thickness 104 μm and dimensions 21 mm by 11 mm was cast on a copper substrate. The plot also includes images of the film obtained at various times during the drying process.

if σ_o is constant throughout the film; E_s and t_s are respectively the Young's modulus and thickness of the substrate, θ is the deflection angle measured at the tip of the film, and t_f and l_f are respectively the average thickness and length of the drying film.

The measured deflection angle, in our experiments, is corrected for the evaporation of the solvent and the corresponding change in the average height of the film so as to yield the bulk stress induced by particle deformation. Some of the experiments were recorded via a video camera to relate features on the film to the variations in the stress.

3. Experiments

As noted earlier by Petersen et al.,[23] the present experimental technique results in a delay of approximately 1 to 2 min between the application of the coating and the start of data acquisition. As a result, the measured deflection deviates from the true value by a constant that corresponds to the net deflection experienced by the substrate before the start of the data acquisition. Because this constant value cannot be ascertained experimentally, the measured values were extrapolated to zero time to determine the shift factor. In almost all cases, except for very thin films, the magnitude of this shift factor was negligible.

Large Particles. Figure 1 presents the bulk stress (1), rendered dimensionless with the characteristic capillary pressure ($2\gamma/R_o$), for PPG342 of initial particle volume fraction 0.50 as a function of dimensionless time, $\hat{t} \equiv (t/t_{evap})$, where γ is the air−water interfacial tension and R_o is the particle radius. Here, time has been rendered dimensionless with the total evaporation time (t_{evap}) such that $\hat{t} = 1$ corresponds to the end of the drying process. A wet film of size 10 mm by 20 mm and of initial average film thickness 104 μm was cast on a copper substrate. In addition to the stress measurements, the plot also includes images of the film that were taken at various times during drying. As reported earlier,[24] in the initial stages of the drying process (before these images were taken) two distinct domains, consisting of an outer saturated region containing packed particles and an inner region of fluid dispersion region, are visible. Since the particles are sufficiently large and the film dimensions are small, water is easily convected from the central dilute domain to the outer edges of the film. As a result, the film remains saturated everywhere and no dry domain forms. Experiments with films of dimensions larger than 30 mm showed the presence of all the three domains.

During the initial phase of drying ($0 \le \hat{t} \le 0.46$), the stress increase is gradual although small fluctuations are noticeable. With continued evaporation, the dilute dispersion domain shrinks in size and results in a dimple at the center of the film ($\hat{t} = 0.46$). The film, at this stage, appears homogeneous and is saturated with the solvent. This also coincides with the steep increase in the stress which, in contrast to the earlier phase, is devoid of fluctuations. The stress reaches a maximum at $\hat{t} = 0.48$. The subsequent decrease in the stress is accompanied by the appearance of bright streaks in the film. Finally, by $\hat{t} = 0.52$, the stress falls to a negligible value. Closer inspection of the drying films under an optical microscope related the appearance of white streaks to the nucleation and propagation of fine cracks in the film radiating from the dimple. Those experiments also showed clear evidence of some cracks being initiated by bubbles trapped at the surface of the films. Figure 2 shows the nucleation of cracks within a span of 2 s from two (of the three) bubbles in a small section of the film prepared from PPG342 dispersion.

(23) Petersen, C.; Heldmann, C.; Johannsmann, D. *Langmuir* **1999**, *15*, 7745−7751.
(24) Tirumkudulu, M.; Russel, W. B. *Langmuir* **2004**, *20*, 2947−2961.

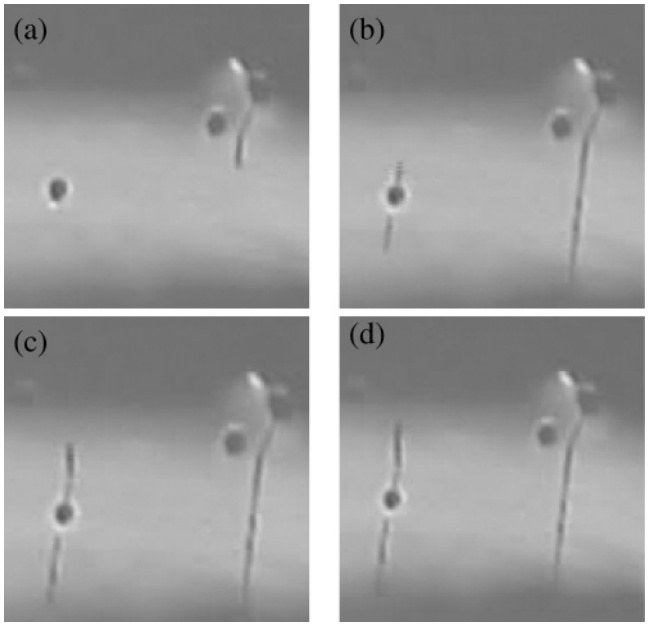

Figure 2. Sequence of images showing the nucleation of cracks and the subsequent propagation of cracks from bubbles trapped at the surface of a wet film that were prepared from the PPG342 dispersion of $\phi_o = 0.32$. The time interval between images (a) and (d) is approximately 2 s. The film was cast on a glass substrate.

Apparently, the nucleation of a crack at the upper most bubble in the image relieved the stress in its vicinity sufficiently to suppress crack formation at the neighboring bubble. Shortly afterward a crack propagates from the third bubble located slightly farther away. We note, however, that cracks also nucleated at sites that appeared to be free of bubbles, although tiny bubbles or flaws of the order of a few particles, which are not resolved by the optical microscope, could be responsible.

As the cracks propagate, the brighter regions observed in Figure 1 grow from both faces of the cracks to encompassed almost the entire film. Such optical contrast could be caused either by the water front receding laterally away from the crack faces or by the debonding from the substrate. To clarify this, thin films of PPG342 dispersion were cast on glass substrates to allow observations from underneath. Figure 3 shows four images acquired at different times during crack propagation. Although the morphology of the film differs from that observed in Figure 1, a streak of brightness appears along the centerline and expands over time to fill almost the entire film. Interestingly, the edge of the film retains the dark contrast observed at the start of the experiment, except for individual fingers reaching outward, even when all the water has evaporated. These results convince us that the change in contrast observed during the crack propagation signals extensive debonding of the film everywhere except at the edges where the thickness suppresses cracking and debonding. These results support the conclusions of Chiu and Cima,[15] who observed that cracking in a film was not initiated at the edge but a small distance into the film. On removal of the debonded film, a scanning electron microscope image (Figure 4a) of the substrate reveals a monolayer of particles coating the substrate. Thus the debonding of films cast on copper substrates does not occur at the particle-substrate interface but represents failure in the first few particle layers. In closing, we note that weight loss experiments revealed a constant net evaporation rate during the drying process, unaffected by the cracks or debonding.

Experiments performed with GMA610 dispersions revealed similar stress profiles and cracks. A plot of the peak stress as a function of the corresponding (average) film thickness scaled on particle diameter for PPG342 ($\phi_o = 0.50$ and 0.38) and GMA610 ($\phi_o = 0.49$) dispersions in Figure 5 reveals comparable values especially at small film thickness ($N < 100$). The magnitudes of 0.1−1.0 times $2\gamma/R_o$ are consistent with the bulk stress originating from the capillary pressure induced by the liquid menisci pulled down between the particles as water evaporates. The peak stress decreases with increasing film thickness suggesting

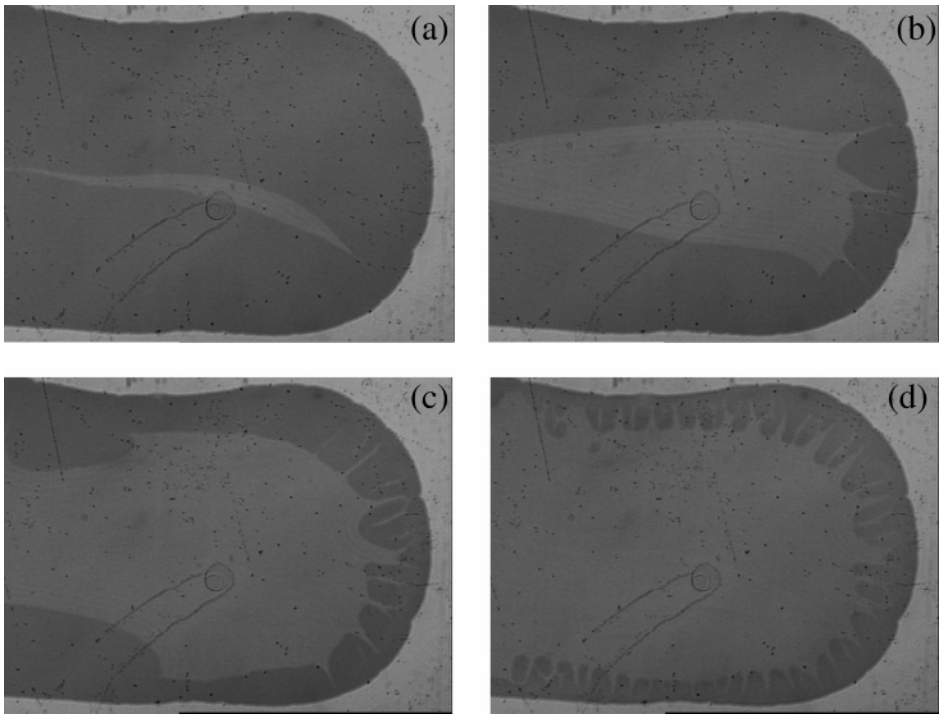

Figure 3. Sequence of images showing the debonding observed from underneath the glass substrate for a film prepared from the PPG342 dispersion of $\phi_o = 0.32$.

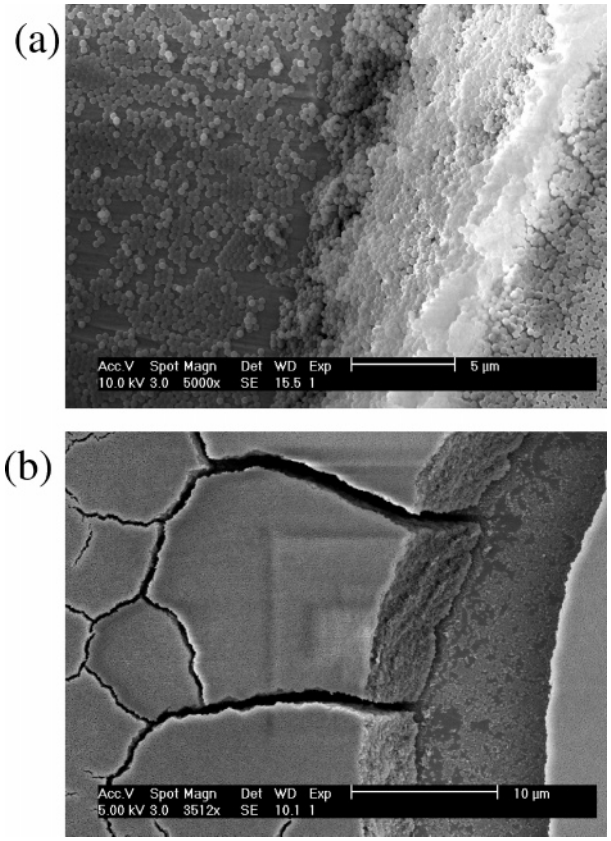

Figure 4. Images revealing the presence of a thin layer of particles on the copper substrate after the films prepared from (a) PPG342, and (b) PMMA95 dispersions have debonded.

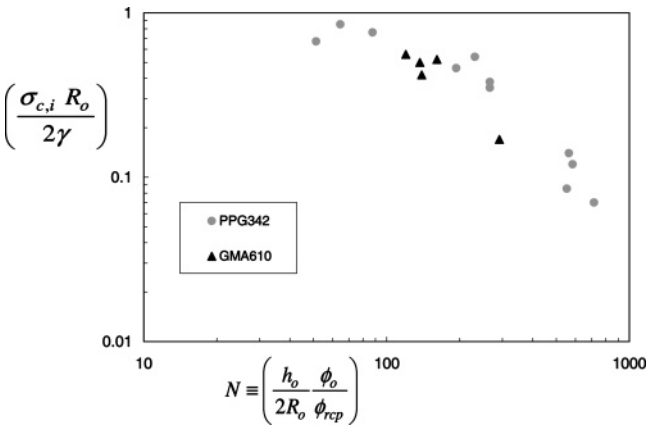

Figure 5. Plot of the maximum stress measured as a function of the dimensionless film thickness for PPG342 and GMA610 dispersions.

that the thinner films sustain larger tensile stresses before cracking in agreement with the findings of Chiu and Cima.[15] We also observed that, irrespective of the film height and initial particle concentration, the stress for both dispersions peaked when the average particle fraction in the film was approximately 0.69, i.e., $\hat{t} \approx (0.69 - \phi_o)/(1 - \phi_o)0.69$.

Small Particles. Next, a plot of the stress profile for the PMMA95 dispersion cast on the copper substrate as a wet film of volume fraction 0.50 and average thickness 97 μm is presented in Figure 6. In contrast to the results obtained with the larger particles, cracks appear close to the edge and propagate toward the center, even while fluid dispersion remains. The bulk stress increases at the start of the drying process but the propagation of the cracks from the edges causes it to decrease beyond $\hat{t} = 0.3$. The crack spacing is surprisingly constant in the lower half of the film and is slightly smaller than observed in the upper half. In addition to the previously observed dilute dispersion and saturated regions visible at $\hat{t} = 0.2$ and 0.35, two more distinct regions with respectively translucent and cloudy white bands appear near the outer edges of the film at $\hat{t} = 0.35$ and 0.40. Within a short time ($\hat{t} \sim 0.4-0.5$), the front separating the cloudy region from the translucent region sweeps across the entire film causing the bulk stress to fall to a minimum at $\hat{t} \sim 0.5$. Immediately thereafter a transparent front appears at the edge of the film ($\hat{t} \sim 0.5$) and the bulk stress begins to rise. The disappearance of the cloudy domain, as the fronts from top and bottom reach the centerline, coincides with the end of drying ($\hat{t} = 1$). Therefore, we feel that the cloudy appearance arises from only partial saturation as the water front recedes from the surface into the film, with the longer persistence in the upper half indicating a somewhat greater thickness. Interestingly, the increase in stress beyond $\hat{t} = 1.0$ occurs in the presence of cracks after all the water has evaporated. We attribute this gradual increase in the stress within the dry regions of the film to the retarded elastic deformation of the particles in response to van der Waals attractions, or capillary forces due to shrinking menisci at the contact point between spheres, that at least partially close the voids in the packed layer and increase the transparency of the film. Though the van der Waals force and the capillary force (due to condensation) are of the same order, the former seems more likely if the capillary force is no stronger than in the saturated phase. The cloudy to transparent transition observed in all films of 95 nm particles was accompanied in some cases by a decrease in the stress, which may arise from debonding of the film.

Further insight can be gained by observing the drying of a thin film cast from a *more* dilute PMMA dispersion and simultaneously recording the weight loss as a function of time. Figure 7 presents images for a wet film of thickness, 280 μm, and initial particle concentration, 0.20, cast on a copper substrate. The first three images clearly show the presence of all the five domains observed in the previously discussed experiment. Regions marked A and B correspond to respectively the dilute dispersion and the close-packed saturated regions, while C and D are reminiscent of respectively the translucent, partially saturated, and cloudy dry but porous domains. Finally, the outermost transparent region, E, corresponds to the fully dry state in which the particles deform under van der Waals forces to induce stress in the film. With time, the fronts separating the domains propagate toward the center. Interestingly, toward the end of the drying process, the transparent domain debonded from the substrate (Figure 7d). The corresponding substrate weight data in Figure 8 indicates that the evaporation rate remains constant through most of the drying process, decreasing slightly only close to the end. Thus, the appearance of different domains with varying water content during the drying process does not decrease the evaporation rate. On removing the debonded film, SEM images (Figure 4b) of the substrate revealed a thin layer of particles adhering to the substrate, as for the films cast from PPG342 dispersions.

In the following section, we develop a model based on the stress−strain relation proposed by Routh and Russel[25] to predict the peak stresses and crack spacing for comparison with the observations.

(25) Routh, A. F.; Russel, W. B. *AIChE J.* **1998**, *44* (9), 2088−2098.

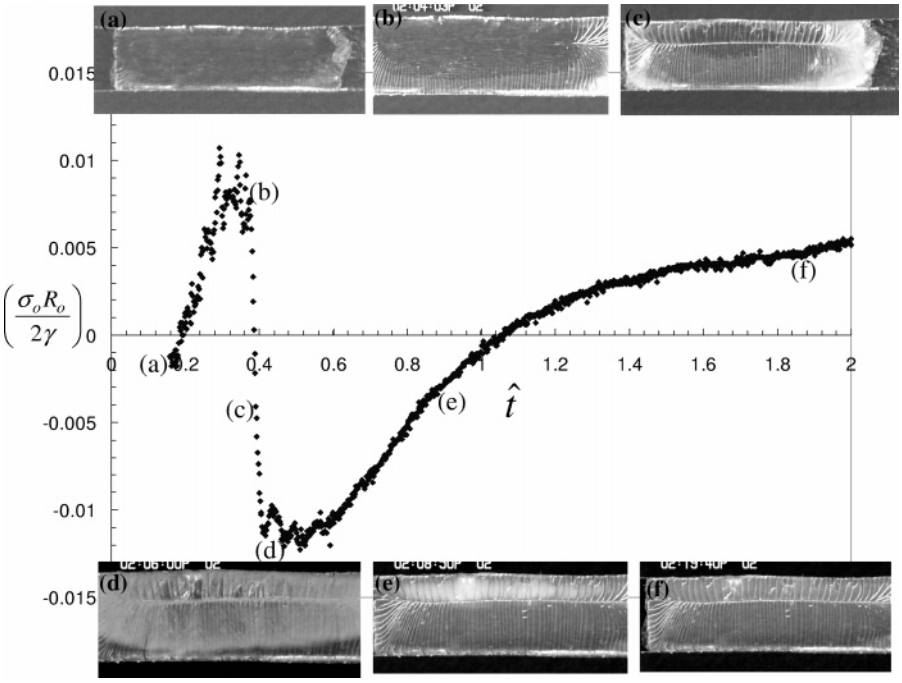

Figure 6. Plot of the dimensionless stress measured for a PMMA95 dispersion of $\phi_o = 0.50$ as a function of dimensionless time, $\hat{t} \equiv tE_o/h_o(1 - \phi_o)$, where E_o is the average evaporation rate. A wet film of average thickness 97 μm and dimensions 12.8 mm by 6.7 mm was cast on a copper substrate. The plot also includes images obtained at various times during the drying process.

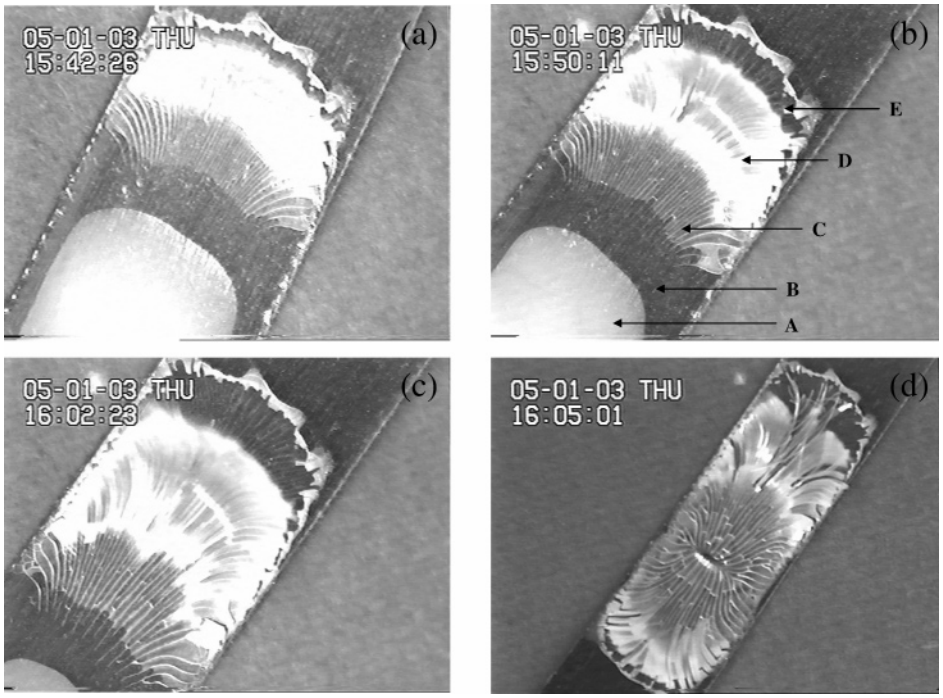

Figure 7. Sequence of images showling the presence of five different domains in drying of a thin film prepared from a PMMA95 dispersion of $\phi_o = 0.20$. Here, a wet film of thickness 230 μm and dimensions 19 mm by 7 mm was cast on a copper substrate.

4. Model

The problem under discussion is somewhat analogous to the cracking of thin elastic films under residual tensile stress bonded to a rigid substrate. Applying the well-known Griffith's criterion for brittle fracture, which balances the elastic energy recovered by crack propagation against the increased surface energy due to creation of new surface, Evans et al.[26] show that the stress at cracking varies inversely with the square root of the film thickness (see Figure 5) for a film and substrate having identical elastic properties. For the general case of dissimilar elastic properties, Beuth[18] calculated the steady-state mode I energy release rate, $\mathcal{G}_I$, for the channeling of an isolated crack across a thin film as

$$\mathcal{G}_I = \frac{1}{2}\frac{{\sigma_o}^2 h}{\bar{E}}\pi g(\alpha, \beta) \tag{2}$$

where σ_o is the far field stress, h is the film thickness, $\bar{E}$ is the thin film plane strain tensile modulus, and $g(\alpha, \beta)$ is the nondimensional integral of the crack opening displacement. The values of the material dependent "Dundurs" parameters are $\alpha = -1$ and $\beta = 0$ for a very

compliant film bonded to a rigid substrate, such as considered here, such that $g(-1, 0) = 0.8153$.

Xia and Hutchison[19] have recently proposed a simplified two-dimensional model of a film bonded to an elastic substrate to treat various complications related to cracking. Starting from a plane stress formulation to describe the in-plane deformation of the film in the presence of cracks, they calculate the energy release rate for the steady-state propagation of a single isolated crack. The shear stress due to interaction between the film and the substrate was assumed to be proportional to the average lateral displacement divided by the film thickness with the proportionality constant calibrated by equating the resulting energy release rate to the exact numerical solution derived by Beuth.[18] This methodology then allows a simpler analysis of more complex crack configurations. While Beuth[18] considers an infinitely thick substrate, Vlassak[27] solved the elastic plane strain problem exactly for a crack in a coating on a substrate of finite thickness to show that the energy release rate becomes independent of substrate thickness in the limit of a very compliant coating (as in our case).

Our analysis follows the methodology outlined by Xia and Hutchinson[19] but employs the constitutive relation proposed by Routh and Russel[6] for a packed array of elastic particles saturated with water. The RR model considers the viscoelastic deformation of a pair of particles in the shape of truncated spheres and relates the interfacial tension between the particle and the surrounding solvent (γ_{ps}) and the external force (F) due to contacting neighbors to the particle strain (ϵ_R),

$$\frac{F}{\pi R_o^{\,2}}\left[1 - \frac{\epsilon_R}{2} + \frac{\epsilon_R^{\,2}}{8}\right] + \frac{\gamma_{ps}}{R_o}\left[\epsilon_R - \frac{5}{4}\epsilon_R^{\,2}\right] = \int_0^t G(t-t')\,\frac{\mathrm{d}}{\mathrm{d}t'}(\epsilon_R^{\,2})\,\mathrm{d}t' + \mathcal{O}(\epsilon_R^{\,3}) \quad (3)$$

where G is the stress relaxation modulus of the particles. The macroscopic stress−strain relation is obtained by volume averaging the force dipoles induced in each pair of particles over all possible orientations and adding the contributions from the capillary pressure in the water P as

$$\sigma_{ij} = \delta_{ij}\left\{-P - \frac{M\phi_{rcp}}{\frac{4}{3}\pi R_o^{\,3}}\left[\frac{\pi R_o^{\,2}\gamma_{ps}}{20}(\epsilon_{mm}^{\,2} + 2\epsilon_{mn}\epsilon_{nm}) + \frac{\pi R_o^{\,3}}{105}\int_{-\infty}^{t} G(t-t')\frac{\mathrm{d}}{\mathrm{d}t'}(\epsilon_{mm}^{\,2} + 2\epsilon_{mn}\epsilon_{nm})\,\mathrm{d}t'\right]\right\} - \frac{M\phi_{rcp}}{\frac{4}{3}\pi R_o^{\,3}}\left\{\frac{\pi R_o^{\,2}\gamma_{ps}}{15}(\epsilon_{mm}\epsilon_{ij} + 2\epsilon_{im}\epsilon_{mj}) + \frac{4\pi R_o^{\,3}}{105}\int_{-\infty}^{t} G(t-t')\frac{\mathrm{d}}{\mathrm{d}t'}(\epsilon_{mm}\epsilon_{ij} + 2\epsilon_{im}\epsilon_{mj})\,\mathrm{d}t'\right\} \quad (4)$$

Here ϵ_{ij} is the macroscopic stress tensor, P is the capillary pressure, ϕ_{rcp} is the random close packing concentration, and M is the number of contacting neighbors.

(26) Evans, A.; Drory, M.; Hu, M. *J. Mater. Res.* **1988**, *3*, 1043−1049.
(27) Vlassak, J. J. *Int. J. Fract.* **2003**, *119/120*, 299−323.
(28) Donev, A.; Cisse, I.; Sachs, D.; Variano, E.; Stillenger, F.; Connelly, R.; Torquato, S.; Chaikin, P. *Science* **2004**, *303*, 990−993.

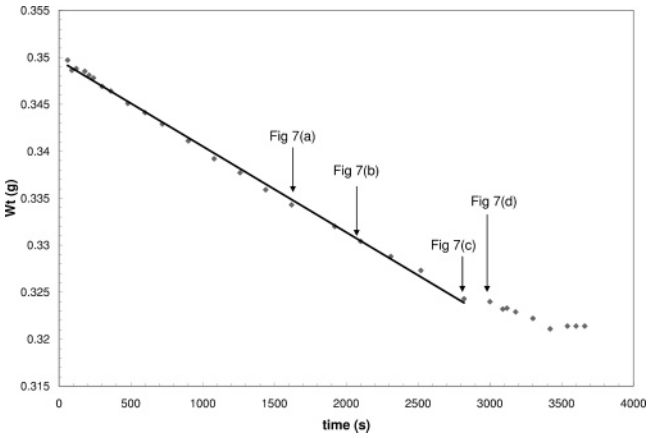

Figure 8. Plot presenting the weight loss experiment as a function of dimensionless time for the experiment presented in Figure 7.

For the case of elastic particles, where the relaxation modulus is simply, $G(t-t') \equiv G$, and the particle−solvent interfacial tension does not contribute to particle deformation, we obtain

$$\sigma_{ij} = \delta_{ij}\left\{-P - \frac{1}{140}MG\phi_{rcp}(\epsilon_{mm}^{\,2} + 2\epsilon_{mn}\epsilon_{nm})\right\} - \frac{1}{35}MG\phi_{rcp}\{\epsilon_{mm}\epsilon_{ij} + 2\epsilon_{im}\epsilon_{mj}\} \quad (5)$$

When water evaporates from a saturated film ($\phi \geq \phi_{rcp}$) that is bonded to the substrate, the induced capillary stresses cause the film to compact/consolidate in the direction perpendicular to the plane of the film. Thus the strain *before* the appearance of the crack is $\epsilon_{ij} = -\epsilon_o\delta_{3i}\delta_{j3}$, where "3" is the direction perpendicular to the plane of the film. The constraint imposed by the substrate induces a biaxial stress in the plane of the film, $\sigma_{11} = \sigma_{22} = \sigma_o$. Since we are interested in the energy change induced on the propagation of cracks, we perturb the stress, pressure, and strain about their initial (pre-crack) state with dashed quantities reflecting the changes,

$$\epsilon_{ij} = -\epsilon_o\delta_{3i}\delta_{j3} + \epsilon_{ij}', \quad P = P^o + P', \quad \sigma_{ij} = \sigma_{ij}^{\,o} + \sigma_{ij}'$$

where

$$\sigma_{ij}^{\,o} = -P^o\delta_{ij} - \frac{3}{140}MG\phi_{rcp}(\epsilon_o)^2(\delta_{ij} + 4\delta_{3i}\delta_{j3})$$

$$P^o = -\frac{3}{28}MG\phi_{rcp}(\epsilon_o)^2$$

$$\sigma_{11}^{\,o} = \sigma_{22}^{\,o} = \sigma_o = \frac{3}{35}MG\phi_{rcp}(\epsilon_o)^2 \quad (6)$$

Next, the expressions involving the strains are expanded in terms of ϵ_o and ϵ_{ij}' as

$$\epsilon_{mm}^{\,2} = (-\epsilon_o + \epsilon_{mm}')^2 = (\epsilon_o)^2 - 2\epsilon_{mm}'\epsilon_o + \epsilon_{mm}'^2$$

$$\epsilon_{mm}\epsilon_{ij} = (\epsilon_o)^2\delta_{3i}\delta_{j3} - \epsilon_o\epsilon_{ij} - \epsilon_o\epsilon_{mm}'\delta_{3i}\delta_{j3} + \epsilon_{ij}'\epsilon_{mm}'$$

$$\epsilon_{im}\epsilon_{mj} = (\epsilon_o)^2\delta_{3i}\delta_{j3} - \epsilon_o\epsilon_{i3}'\delta_{3j} - \epsilon_o\epsilon_{3j}'\delta_{3i} + \epsilon_{im}'\epsilon_{mj}'$$

We retain the linear terms so as to obtain a constitutive relation that is similar in form to the standard equations of linear elasticity,

$$\sigma_{ij}' = \delta_{ij}\left\{-P' - \frac{1}{70}MG\phi_{rcp}\epsilon_o(\epsilon_{mm}' + 2\epsilon_{33}')\right\} + \frac{1}{35}MG\phi_{rcp}\epsilon_o\{\epsilon_{ij}' + \epsilon_{mm}'\delta_{3i}\delta_{j3} + 2\epsilon_{i3}'\delta_{3j} + 2\epsilon_{3j}'\delta_{3i}\} \quad (7)$$

Now, we consider an isolated semi-infinite crack oriented along the x_1 axis so that far ahead of the crack tip, the film is in its base state (Figure 9). However, far behind the crack tip, i.e., $x_1 \rightarrow -\infty$, all quantities should be independent of x_1 (i.e., $\partial/\partial x_1 = 0$). The height averaged normal stress in the "3" direction,

$$\langle\sigma_{33}'\rangle = -\langle P'\rangle + \frac{3}{70}MG\phi_{rcp}[\langle\epsilon_{22}'\rangle + 5\langle\epsilon_{33}'\rangle]$$

must be zero because of the free surface, so

$$\langle\epsilon_{33}'\rangle = \frac{14}{3\phi_{rcp}\epsilon_o MG}\left(\langle P'\rangle - \frac{3}{70}MG\phi_{rcp}\epsilon_o\langle\epsilon_{22}'\rangle\right) \quad (8)$$

Thus

$$\langle\sigma_{11}'\rangle = -\frac{4}{5}\langle P'\rangle + \frac{1}{175}MG\phi_{rcp}\epsilon_o\langle\epsilon_{22}'\rangle \quad (9)$$

$$\langle\sigma_{22}'\rangle = -\frac{4}{5}\langle P'\rangle + \frac{6}{175}MG\phi_{rcp}\epsilon_o\langle\epsilon_{22}'\rangle \quad (10)$$

The height averaged equilibrium equation in the plane of the film (equivalent to the generalized plane stress formulation) is given by

$$\frac{\partial\langle\sigma_{22}'\rangle}{\partial x_2} = \left.\frac{\sigma_{23}'}{h}\right|_{x_3=0} \quad (11)$$

Generally, the plane stress approximation applies to thin plates with negligible forces acting on its surfaces, so the terms on the right-hand side of (11) would not exist. Since they are critical to our situation, we follow Xia and Hutchinson[19] in approximating $\epsilon_{23}'(x_3 = 0) = \bar{k}^2\langle u_2'\rangle/2h$ and then calibrate the solution for an isolated crack in a bonded linearly elastic film against the exact one to determine $\bar{k}$. Substituting this approximation for perturbed stress yields

$$-\frac{4}{5}\frac{\partial\langle P'\rangle}{\partial x_2} + \frac{6}{175}MG\phi_{rcp}\epsilon_o\frac{\partial^2\langle u_2'\rangle}{\partial {x_2}^2} = \frac{3}{70}MG\phi_{rcp}\epsilon_o\frac{\bar{k}^2}{h^2}\langle u_2'\rangle \quad (12)$$

The equivalent plane stress equilibrium relation for a linear elastic material obeying Hooke's law is given by

$$\frac{E}{1-\nu^2}\frac{\partial^2\langle u_2'\rangle}{\partial {x_2}^2} = \frac{1}{2}\frac{E}{1+\nu}\frac{\bar{k}^2}{h^2}\langle u_2'\rangle \quad (13)$$

Xia and Hutchinson[19] have shown that (13) can model effectively the cracking of bonded elastic films as long as the energy release rate for the semi-infinite crack is set to equal the exact numerical solution obtained by Beuth.[18] Thus $\bar{k}$ must satisfy

$$\sqrt{\frac{70\bar{E}}{3MG\phi_{rcp}\epsilon_o\bar{k}^2}} = \frac{\pi}{2}g(\alpha, \beta); \quad \bar{E} = \frac{E}{1-\nu^2} \quad (14)$$

where E is the Young's modulus and ν is the Poisson's ratio. The above case is equivalent to the cracking of stressed latex film in the absence of water ($P' = 0$).

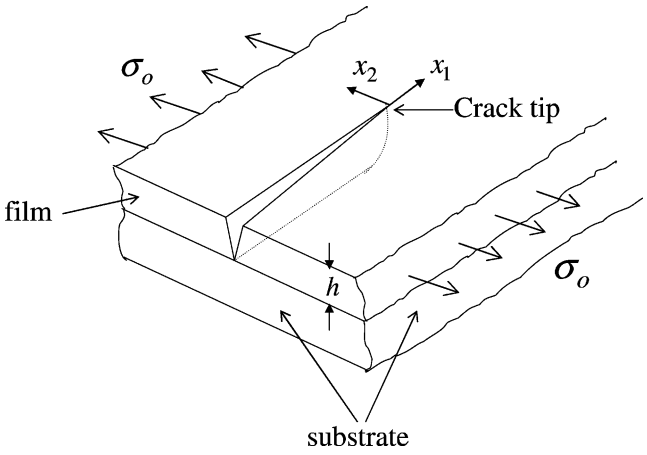

Figure 9. Schematic diagram of an isolated crack propagating across the film.

Consequently, comparing equation (13) with equation (12) for the case $P' = 0$ yields the Young's modulus, $E = MG\epsilon_o\phi_{rcp}/30$, and Poisson's ratio, $\nu = 1/6$, of the dry elastic porous network. On substituting the expression for E and ν in (14), we arrive at a simple expression for the spring constant $\bar{k}$,

$$\bar{k}^2 = \frac{4}{5[(\pi/2)g(-1, 0)]^2} \approx 0.488 \quad (15)$$

For propagation of an isolated semi-infinite crack in a saturated film under tension the equilibrium equation (12) relates the two unknowns, $\langle u_2'\rangle$ and $\langle P'\rangle$. Thus we need a second relation characterizing the fluid flow in the porous structure during crack propagation. At short times, just after the appearance of the crack, fluid has no time to flow through the network, so the film must deform incompressibly. The perturbed pressure is obtained by setting the trace of the strain to zero (*short time limit*). On the other hand, on long enough time scales fluid flow allows the perturbed pressure to relax to zero (*long time limit*). The ensuing analysis treats both limits in calculating the total elastic energy released during the propagation of a semi-infinite isolated crack.

4.1. Short Time Limit. On applying the incompressibility condition, $\langle\epsilon'_{33}\rangle = -\langle\epsilon'_{22}\rangle$, the perturbed pressure follows as

$$\langle P'\rangle = -\frac{6MG}{35}\phi_{rcp}\epsilon_o\langle\epsilon_{22}'\rangle \quad (16)$$

Equation 12 can now be solved to yield the displacements

$$\langle u_2'(x_2)\rangle = \frac{h}{\bar{k}}\epsilon_o e^{-\bar{k}x_2/2h}$$

with $\bar{k}$ from (15). The resulting stress and strain components

$$\langle\sigma_{11}'\rangle = -\frac{5}{6}\sigma_o e^{-\bar{k}x_2/2h} = \frac{5}{6}\langle\sigma_{22}'\rangle = -\frac{5}{3\bar{k}}\langle\sigma_{23}'\rangle$$

$$\langle\epsilon_{22}'\rangle = -\frac{\epsilon_o}{2}e^{-\bar{k}x_2/2h} = -\frac{1}{\bar{k}}\langle\epsilon_{23}'\rangle$$

decay with distance ($x_2 \rightarrow \infty$) from the crack.

The stress in the elastic network, $\sigma_{ij,p}$, is related to the volume average stress and the fluid pressure by

$$\sigma_{ij} = \phi_{rcp}\sigma_{ij,p} - (1 - \phi_{rcp})P\delta_{ij}$$

The change in the total elastic energy (per unit surface area of the crack) on the passage of the crack, to the lowest order, is given by

$$\Delta\mathcal{E} = 2\phi_{rcp}\int_0^\infty \{\int_{-\epsilon_o\delta_{3i}\delta_{j3}}^{\langle\epsilon_{ij}\rangle} \langle\sigma_{ij,p}\rangle \, \mathrm{d}\langle\epsilon_{ij}'\rangle\} \, \mathrm{d}x_2, \quad (i,j = 1, 2)$$

$$= 2\int_0^\infty \left\{\sigma_o\langle\epsilon_{22}'\rangle + \frac{1}{2}\langle\sigma_{22}'\rangle\langle\epsilon_{22}'\rangle + \langle\sigma_{23}'\rangle\langle\epsilon'_{23}\rangle\right\} \mathrm{d}x_2$$

$$\Rightarrow \Delta\mathcal{E} = \frac{9}{70}\left[-\frac{1}{\bar{k}} + \frac{\bar{k}}{3}\right]MG\phi_{rcp}h(\epsilon_o)^3 \tag{17}$$

Here, repeated indices imply summation. The first term in (17) represents recovery of energy from the relaxation of the film, while the second term due to the shear deformation increases the total elastic energy. Note that viscous dissipation would retard the relaxation and dissipate energy but would not affect the total elastic recovery.

For equilibrium crack propagation, the total elastic energy recovery must balance the increase in interfacial energy. Since the porous network is saturated with water, the surface energy per unit area corresponds to the interfacial energy between water and air (γ), leaving the balance as

$$\frac{9}{70}\left[-\frac{1}{\bar{k}} + \frac{\bar{k}}{3}\right]MG\phi_{rcp}h(\epsilon_o)^3 + 2\gamma = 0 \tag{18}$$

Substituting for ϵ_o from (6) results in an expression that relates the dimensionless critical stress for an isolated crack ($\sigma_{c,i}$) to the dimensionless film thickness,

$$\frac{\sigma_{c,i}R_o}{2\gamma} = 0.1877\left(\frac{2R_o}{h}\right)^{2/3}\left(\frac{GM\phi_{rcp}R_o}{2\gamma}\right)^{1/3} \tag{19}$$

Here, h corresponds to the height of the film at the time of crack initiation and is related to the bulk strain (ϵ_o) by

$$h = h_{rcp}(1 - \epsilon_o) = (h_o\phi_o/\phi_{rcp})(1 - \epsilon_o)$$

where h_o and ϕ_o are respectively the initial average height and particle fraction of the film and h_{rcp} is the height at random close packing. Since $\epsilon_o \ll 1$, h can be replaced by h_{rcp} in (19) to obtain the critical stress as a function of the initial height. While the application of Griffith's criterion for a linearly elastic material predicts the stress at cracking to vary inversely with square root of the film thickness,[26] the current analysis for a porous film with imbibed liquid predicts a stress that varies inversely with square of the cube root of the film thickness.

4.2. Long Time Limit. At longer times the fluid will flow through the packed particle bed to equilibrate the pressure and the fluid velocity will relax to zero everywhere. Assuming the pressure to equilibrate over times much shorter than required for significant evaporation gives

$$\frac{\partial\langle P'\rangle}{\partial x_2} = 0 \quad \text{with} \quad \langle P'\rangle \to 0 \quad \text{as} \quad x_2 \to \infty$$

$$\Rightarrow \langle P'\rangle = 0$$

We apply the same boundary conditions as before to solve the equilibrium relation and arrive at the displacement,

$$\langle u_2'\rangle = \sqrt{5}\,\frac{h\epsilon_o}{\bar{k}}\mathrm{e}^{-\sqrt{5}\bar{k}x_2/2h} \tag{20}$$

the strain,

$$\langle\epsilon_{22}'\rangle = -\frac{5}{2}\epsilon_o\mathrm{e}^{-\sqrt{5}\bar{k}x_2/2h} \tag{21}$$

and the bulk stresses,

$$\langle\sigma_{22}'\rangle = -\sigma_o\mathrm{e}^{-\sqrt{5}\bar{k}x_2/2h} = 6\langle\sigma_{11}'\rangle = -\frac{2}{\bar{k}\sqrt{5}}\langle\sigma_{23}'\rangle$$

In the absence of a perturbed liquid pressure, the perturbed particle stress is simply

$$\sigma_{ij,p}' = \frac{\sigma_{ij}'}{\phi_{rcp}}$$

leaving the change in the elastic energy (per unit volume) accompanying the advance of the crack tip as

$$\Delta\mathcal{E} = 2\int_0^\infty \left\{\phi_{rcp}\sigma_o\langle\epsilon_{22}'\rangle + \frac{1}{2}\langle\sigma_{22}'\rangle\langle\epsilon_{22}'\rangle + \langle\sigma_{23}'\rangle\langle\epsilon'_{23}\rangle\right\} \mathrm{d}x_2$$

$$= -\frac{6\sqrt{5}}{35}\left[\frac{\phi_{rcp} - 1/4}{\bar{k}} - \frac{\bar{k}}{4}\right]MG\phi_{rcp}h(\epsilon_o)^3 \tag{22}$$

As before, equating the change in total elastic energy to the increase in surface energy relates the critical stress at cracking, $\sigma_{c,i}$, to the film thickness,

$$\frac{\sigma_{c,i}R_o}{2\gamma} = 0.1023\left(\frac{2R_o}{h}\right)^{2/3}\left(\frac{GM\phi_{rcp}R_o}{2\gamma}\right)^{1/3}\left(\frac{4\phi_{rcp}}{\bar{k}} - \frac{1}{\bar{k}} - \bar{k}\right)^{-2/3} \tag{23}$$

$$\frac{\sigma_{c,i}R_o}{2\gamma} \approx 0.1804\left(\frac{2R_o}{h}\right)^{2/3}\left(\frac{GM\phi_{rcp}R_o}{2\gamma}\right)^{1/3} \tag{24}$$

with $\phi_{rcp} = 0.67$. Interestingly, the predicted dimensionless critical stresses for the short and long time limits differ by less than 5%.

4.3. Multiple Cracks. Since the solutions for the two limits differ little for an isolated crack, we next consider, in detail, only the short time limit to predict the multiple cracks observed in experiments with PMMA95 dispersion. The solution of the single crack can easily be extended to multiple cracks by replacing the boundary condition for $\langle u'_2\rangle$ at infinity by

$$\langle u'_2\rangle|_{x_2=W} = 0$$

where the crack spacing is $2W$. On retaining the remaining boundary conditions, we obtain the displacement as

$$\langle u'_2\rangle = -\frac{h\epsilon_0}{\bar{k}}\frac{\sinh(\bar{k}(x_2 - W)/2h)}{\cosh(\bar{k}W/2h)} \tag{25}$$

and strain as

$$\langle\epsilon_{22}'\rangle = -\frac{\epsilon_o}{2}\frac{\cosh(\bar{k}(x_2 - W)/2h)}{\cosh(\bar{k}W/2h)} \tag{26}$$

Note that the strain is symmetric about $x_2 = W$. Following

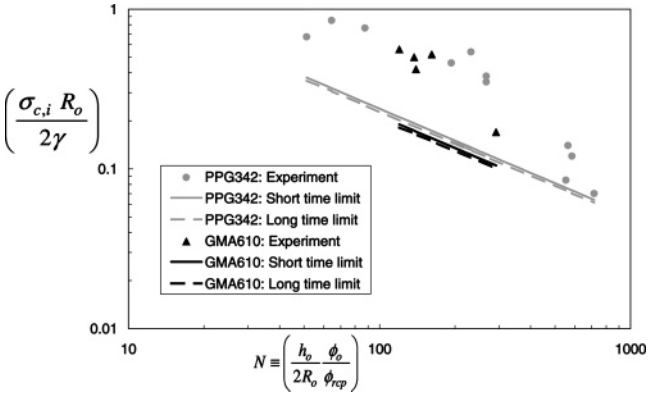

Figure 10. Critical stress (at cracking) for films cast from PPG and GMA dispersions compared with the predictions of the plane stress approximation.

the steps outlined before for a single crack yields the energy release rate for multiple cracks as

$$\Delta\mathcal{E} = -\frac{3}{2}h\sigma_o\epsilon_o\left(\frac{1}{\bar{k}} - \frac{\bar{k}}{3}\right)\left\{\tanh\left(\frac{\bar{k}W}{2h}\right) - \left(\frac{1-\bar{k}^2}{3-\bar{k}^2}\right)\frac{\bar{k}W/2h}{\cosh^2[\bar{k}W/(2h)]}\right\} \quad (27)$$

As expected, the above equation reduces to the energy release rate for a semi-infinite isolated crack (17) in the limit $W \to \infty$. Equating the elastic energy released to the increase in the interfacial energy, in contrast to an isolated crack, relates the critical stress and the crack spacing to the film height, but does not determine either uniquely.

Recall that, for PMMA95 dispersions, the cracks nucleate at the film edges while the central region still contains dilute dispersion. Since the measured stress in such cases (Figure 6) represents an integral over the outer dry domain and the inner fluid domain, both of which are inhomogeneous, we were unable to measure the stress associated with crack propagation. However, the critical stress associated with multiple cracks is higher than that for a single crack, so we substitute $\sigma_{c,m} = K\sigma_{c,i}$ ($K > 1$) in (27) to relate the crack spacing to the film thickness as

$$\frac{1}{K^{3/2}} = \begin{cases} \tanh\left(\frac{\bar{k}W}{2h}\right) - \frac{\bar{k}W/2h}{\cosh(\bar{k}W/2h)}\left[\frac{\bar{k}^2-1}{\bar{k}^2-3}\right] & \text{short time} \quad (28) \\ \tanh\left(\frac{\sqrt{5}\bar{k}W}{2h}\right) - \frac{\sqrt{5}\bar{k}W/2h}{\cosh(\sqrt{5}\bar{k}W/2h)}\left[\frac{\bar{k}^2-1}{\bar{k}^2+1-4\phi_{rcp}}\right] & \text{long time} \quad (29) \end{cases}$$

5. Comparison with Experiments

Figure 10 compares the measured critical stress for the PPG342 and GMA610 dispersions with that predicted by the short and long time limits. The other parameters needed are listed in Table 1. While the observed stresses are approximately three times those predicted by the two limits, the predicted trend agrees well with the measured values. These results also suggest that the dynamics of crack propagation are described equally well by either the incompressibility condition or the uniform pressure condition. Interestingly, for a solid linear elastic film the critical stress has an inverse square dependence on film height,[26] which is a weaker dependence than that predicted here. Both the model and the data indicate that thicker films crack at lower stresses.

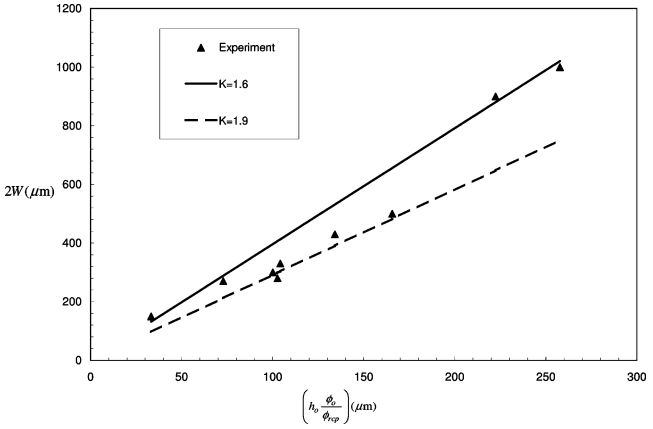

Figure 11. Observed crack spacing for films cast from PMMA95 dispersions compared with the predictions of the plane stress approximation.

Equation (6) relates the critical stress and the corresponding capillary pressure by a simple relation, $P^o = -(5/4)\sigma_o$, allowing us to compare the theoretical maximum in the capillary stress with the measured values. Geometrical arguments dictate the maximum dimensionless capillary pressure $P^oR_o/(2\gamma_{wa})$ for menisci formed within an ordered array of spheres to lie between 2 and 5. Indeed the measured values vary between 0.1 and 1.0 over the range of film thicknesses in this study, suggesting the cracking is not driven by the recession of the air−water interface into the film.

Figure 11 compares the observed crack spacing as a function of film height for the PMMA95 dispersion with that predicted by (28) for two values of K greater than unity, since the stress in the film must exceed the critical stress for an isolated crack. The measured crack spacing increases approximately linearly with film thickness, consistent with the predictions for $K = 1.6-1.9$. For comparison the value of K can be estimated from experiments for comparison by determining the capillary pressure at the crack tip ($P_{\text{crack tip}}$). A simple mass balance for water transport across a drying porous film of uniform thickness gives

$$P_{\text{crack tip}} = \frac{\mu\dot{E}_o}{k_p h}(L_c^2 - L^2)$$

where μ is the viscosity of water, $k_p = 2R_o^2(1-\phi_{rcp})^2/(75\phi_{rcp}^2)$ is the permeability of the film at random close packing, and L and L_c are respectively the length of the saturated region and the distance between the crack tip and the saturated−dry film front. The value of K can then be determined by taking the ratio of the stress at crack tip and the critical stress for an isolated crack under similar conditions. For the experiment shown in Figure 7, the value of K estimated from the clearly visible fronts in panel (c) is around 1.6, in good agreement with the model predictions.

6. Conclusions

Thin films of latex dispersions containing particles of varying sizes and glass transition temperatures were dried under ambient conditions to understand the phenomenon of cracking. Capillary stresses induced during drying were measured via the classical cantilever technique. Films cast from dispersions containing large particles (PPG342

and GMA610) resulted in three domains, namely, a central dilute dispersion domain, an outer dry film and an intermediate saturated film. However, films cast from dispersions containing small particles (PMMA95) became transparent and yielded tensile stresses even when all the water had evaporated. Although the transparency of the final film may be attributed to the small size of the particles, the presence of tensile stress suggests that van der Waals forces are capable of deforming small particles. Closer inspection of the drying films showed that cracks can be nucleated by bubbles trapped at the surface of the film. Propagation of cracks were also accompanied with debonding of the films from the substrates.

The measured critical stresses and the crack spacing were compared with the predictions of a model derived from the constitutive equation proposed by Routh and Russel[6] for drying latex films. Employing the classical Griffith's energy balance concept, we derived a scaling for the critical stresses that agreed well with the experimental values. Both the measured and the predicted crack spacing varied linearly with film height with the observed slope in fair agreement with the predicted values for $K = 1.6-1.9$. An estimate of K from experiments falls within this range.

From the critical stress for cracking and the capillary pressure required to close all the pores via elastic deformation ($\epsilon_o = 0.33$), we can estimate the conditions required to avoid cracking. According to the theory the capillary pressure will form a void free continuous film before cracking occurs if $\sigma_o(\epsilon_o = 0.33) < \sigma_{c,i}$. This translates into a maximum film thickness of $h_{\max} = 361\gamma/GM\phi_{rcp}$. Since the maximum film thickness for forming a crack free film is of the order of 1−10 nm for the dispersions used in this study, a different set of dispersions would be required to confirm the predictions.

Acknowledgment. The work reported here was supported in part by the Petroleum Research Fund and the National Science Foundation (CTS 0120421). The authors thank Dr. W. C. Flood of Rohm & Haas and Dr. K. Takamura of BASF for their generous donations of latex dispersions.

LA048298K